

pubs.acs.org/JPCC Article

Elucidating the Influence of Metal Surface Composition on Organic Adsorbate Binding Using Active Particle Dynamics

Benjamin Greydanus, J. Will Medlin,* and Daniel K. Schwartz*



Cite This: J. Phys. Chem. C 2023, 127, 1006-1014



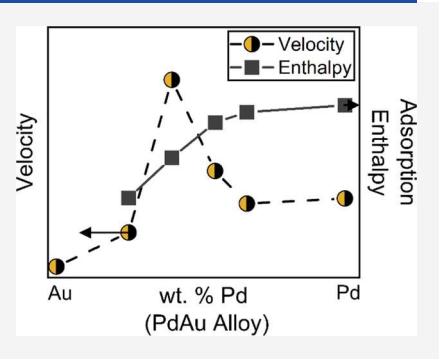
ACCESS I

Metrics & More

Article Recommendations

Supporting Information

ABSTRACT: The adsorption strengths of organic compounds on metal surfaces are sensitive to the metal composition, and they play a central role in many catalytic reactions, helping to control the coverage of the reactant and altering the overall reaction rate. While adsorption energies are straightforward to measure and calculate in vacuum and gas-phase environments, adsorption energetics can be dramatically altered by the presence of solvent in liquid-phase reactions. However, the effects of metal composition on binding strengths in a liquid environment are less well understood, primarily due to the difficulty of accurate *in situ* measurements of organic binding on metal surfaces in the liquid phase. Here, we utilize the motion of active particles in water to probe the adsorption energies of an organic adsorbate (furfural) on a range of metal surfaces (pure Pd, pure Pt, and four PdAu alloy compositions) to elucidate the effect of metal composition. Janus particles with catalytic caps of particular metal compositions all exhibited active motion resulting from



consumption of H_2O_2 ; adsorbate binding was inferred through the decrease in the velocity of active motion and was modeled by a Langmuir adsorption isotherm. The measured adsorption affinities were used to extract the adsorption enthalpy of furfural on the different metals. The Pd surface was found to bind furfural more strongly than the Pt surface by some 10 kJ/mol. Furthermore, the adsorption of furfural on the alloys was found to increase monotonically in magnitude with Pd content. The data reported herein aid the development of accurate understanding of organic adsorption in the presence of solvent and the role of the metal surface in tuning adsorption strengths to optimize catalytic processes in the liquid phase.

1. INTRODUCTION

Supported noble metal heterogeneous catalysts have increasingly been applied for liquid phase production of industrially relevant chemicals. 1,2 However, predicting and controlling the near-surface environment of the catalyst surface under reaction conditions remains challenging, especially for reactions in the condensed liquid phase. The solvent can have complicated interactions with the catalyst, for example, through competitive adsorption to catalyst active sites.³ Furthermore, solvent molecules have been implicated directly in reaction mechanisms through stabilization of key intermediates. The presence of solvent can also change the adsorption strengths of organic species on the metal catalyst surface. While understanding these affinities (and related adsorption strengths) is critical to rational catalyst design, there is a need for techniques capable of probing the interplay of solvent, adsorbate, and catalyst surface. Furthermore, adsorbate binding is commonly interpreted using scaling relations to help predict adsorption energies on different surfaces and to guide development of optimal catalysts for a variety of reactions. While binding strength studies to determine scaling relations for oxygenated adsorbates on metal surfaces are commonly performed in vacuum, many catalytic processes are conducted in liquid solvent environments and the interactions of metal surface, adsorbate, and solvent can drastically modulate the energetics compared to vacuum. This necessitates correction of any predicted vacuum or gas-phase binding energies to account for the so-called solvent effect; however, the lack of widespread *in situ* techniques to probe binding energetics in the liquid phase complicates full understanding of the solvent energy correction required. In particular, the largely unknown effect of changing metal composition on this solvent energy correction is key to developing scaling relations in the liquid phase.

A growing number of computational and experimental techniques have been employed to better address the shortcomings in the understanding of liquid-phase organic adsorption. Both implicit and explicit computational treatment of the solvent have been used to model solvent-mediated energy differences in the liquid phase. Though powerful tools help predict solvent effects on binding, these large-scale solvent models are computationally costly and often require experimental benchmarking. Consequently, sophisticated experimental techniques have been developed; for example, hydrogen underpotential deposition through cyclic voltamme-

Received: August 19, 2022 Revised: December 21, 2022 Published: January 9, 2023





try was used to estimate the coverage of organics on Pt and Rh wires. These results were complemented by X-ray absorption spectroscopy (XAS) to directly probe the hydrogen surface coverage on the Pt surface. Both techniques involve application of a potential to the surface, which may alter adsorption energetics relative to an uncharged surface.

Here, we utilize self-propelled active particles for quantification of the key parameters of organic binding on metal surfaces in the liquid phase. Active particles are colloids that convert environmental energy into directed mobility that exceeds Brownian motion. 10 For example, Janus particles with a cap of catalytic metal (typically Pt) move autonomously in a fuel solution of H₂O₂. The Pt sites rapidly decompose H₂O₂. creating an asymmetric chemical gradient that acts to propel the particle. 12 In a previous work, the dependence of active motion on solute concentration was used to quantify adsorption on available metal surface sites. ¹³ Furfural adsorption was studied on a Pt surface to determine key aspects of binding including the affinity, concentrationdependent coverage, and enthalpy of adsorption for furfural on Pt. Here, we investigate the use of other metal compositions including Pd and Pd-containing alloys. Similar to Pt, Pd catalysts are ubiquitous in industry and are widely used to process and upgrade biomass-derived aromatic oxygenates such as furfural. 14,15 Despite their widespread use, trends in furfural binding on Pt versus Pd in vacuum remain unclear 14,16,17 and the solvent is expected to further modulate these adsorption strengths; 18 consequently, the relative binding of furfural on Pt and Pd is largely unknown in the liquid phase.

Alloying metals can yield useful synergistic effects on reactivity and a variety of metal alloys are employed in largescale catalytic processes to produce valuable commodity chemicals.¹⁹ For example, bimetallic alloys of Pd and Au are used as versatile catalysts for a variety of important liquidphase reactions, including alcohol oxidations, nitrate reduction, and direct synthesis of hydrogen peroxide. 20-23 The composition of Pd and Au in the alloy has been shown to have large effects on the catalytic performance in these systems, with some Pd/Au ratios maximizing catalytic performance with volcano-type trends.²⁴ Rational design and selection of appropriate catalyst surfaces to understand and optimize these trends in reactivity is desirable. As with pure metal surfaces, however, the solvent can drastically modulate the binding energetics compared to vacuum and these solvent binding effects on alloyed surfaces are not understood. Therefore, we further seek to extend the measurement of adsorbate binding using active particles to study furfural adsorption on a variable compositional range of Pd and PdAu surfaces to determine the effect of increasing Pd content on the binding of organic compounds in the liquid phase.

Here, furfural adsorption on pure Pd and alloys of PdAu was quantified by synthesizing particles with Janus caps of the different metal compositions. These particles all self-propelled in H_2O_2 fuel solutions due to asymmetric decomposition of the fuel around the metal cap; consequently, decreases in the rate of H_2O_2 decomposition due to competitive binding of furfural manifested as measurable decreases in the particle velocity. This adsorbate-mediated attenuation of particle velocity was exploited to construct apparent adsorption isotherms and to extract the approximate adsorption enthalpy of furfural on the different metals, further elucidating the effect of pure and alloyed metal composition on organic molecule binding in the liquid phase.

2. MATERIALS AND METHODS

An overview of the most pertinent experimental details follows. The reader is referred to the Supporting Information for a more detailed description of the methods.

2.1. Active Particle Synthesis and Characterization. Active particles were synthesized by first spin-coating a suspension of 1 µm particles (carboxylate-modified polystyrene, fluorescent red, Fischer) onto a glass slide at submonolayer concentrations. The immobilized particles were then sputter-coated (Cressington 108Auto) with a ~5 nm layer of metal on the exposed particle hemisphere. A pure Pt sputter target (57 mm diameter, purity 99.95%, Ted Pella) was used to deposit Pt, and a pure Pd sputter target (57 mm diameter, purity 99.9%, Ted Pella) was used to deposit Pd. Alloys of PdAu were sputtered by adhering small gold discs [15.88 mm diameter, purity (99.99%, SurePure Chemetals)] to the Pd target using conductive silver epoxy (CircuitWorks) (schematic shown in Figure S1). The number (1, 2, or 3 discs) and proximity of the gold discs to the center of the Pd sputter target were adjusted to give different ratios of Pd and Au (PdAu 40:60 composition was synthesized using a commercial 40:60 alloy target). The metal layer thickness for each sample was monitored via a Cressington Thickness Monitor. After metal deposition, the particles were liberated from the glass slide by sonication (2-3 min) and redispersed into 2 mL of water [high-performance liquid chromatography (HPLC)grade, \geq 99.9%, Fisher].

Transmission electron microscopy (TEM) was used to confirm the asymmetry of the deposited metal. The composition of the sputtered PdAu alloys was probed two ways: first, energy-dispersive spectroscopy (EDS) was used to analyze the bulk composition (Oxford Instruments Ultim Max EDS system coupled with a Hitachi SU3500 SEM). The metal composition was further probed using low-energy ion scattering spectroscopy (LEIS) (IONTOF) to selectively determine the composition of the outermost atomic layers.

2.2. Imaging Particle Dynamics. Active and passive particle dynamics were imaged using a Nikon N-Storm microscope. The particles were excited using a 647 nm laser line and imaged using a Hamamatsu ORCA-Flash4.0 V2 C11440 camera, a 100× oil immersion objective (NA: 1.45), and a double-helix point spread function (DH-PSF) SPINDLE module (Double Helix LLC, Boulder, calibration shown in Figure S2). An environmental chamber (Okolab Cage Incubator) was used to control the temperature of the particle solution during imaging.

Adsorbate coverage on the metal surface of the particle was tuned by incubating particles with solutions containing varying concentrations of furfural (99%, Sigma-Aldrich) for at least 1 h prior to imaging.

Immediately before imaging, samples were prepared by mixing the particle suspensions (either neat or incubated with varying amounts of furfural) with hydrogen peroxide (30% w/w, Fisher) to form a 10% $\rm H_2O_2$ solution. An aliquot of this solution was introduced to an imaging cell constructed using two cleaned glass slides separated by an adhesive spacer, and the cell was transferred to the microscope for imaging.

Multiple movies (3600 frames, acquisition time of 10 ms) of particle motion were acquired in multiple fields of view, and the dynamics of >50 colloids were imaged at each condition. Passive motion (*i.e.* thermal diffusion) was measured using similar procedures but without the addition of H_2O_2 .

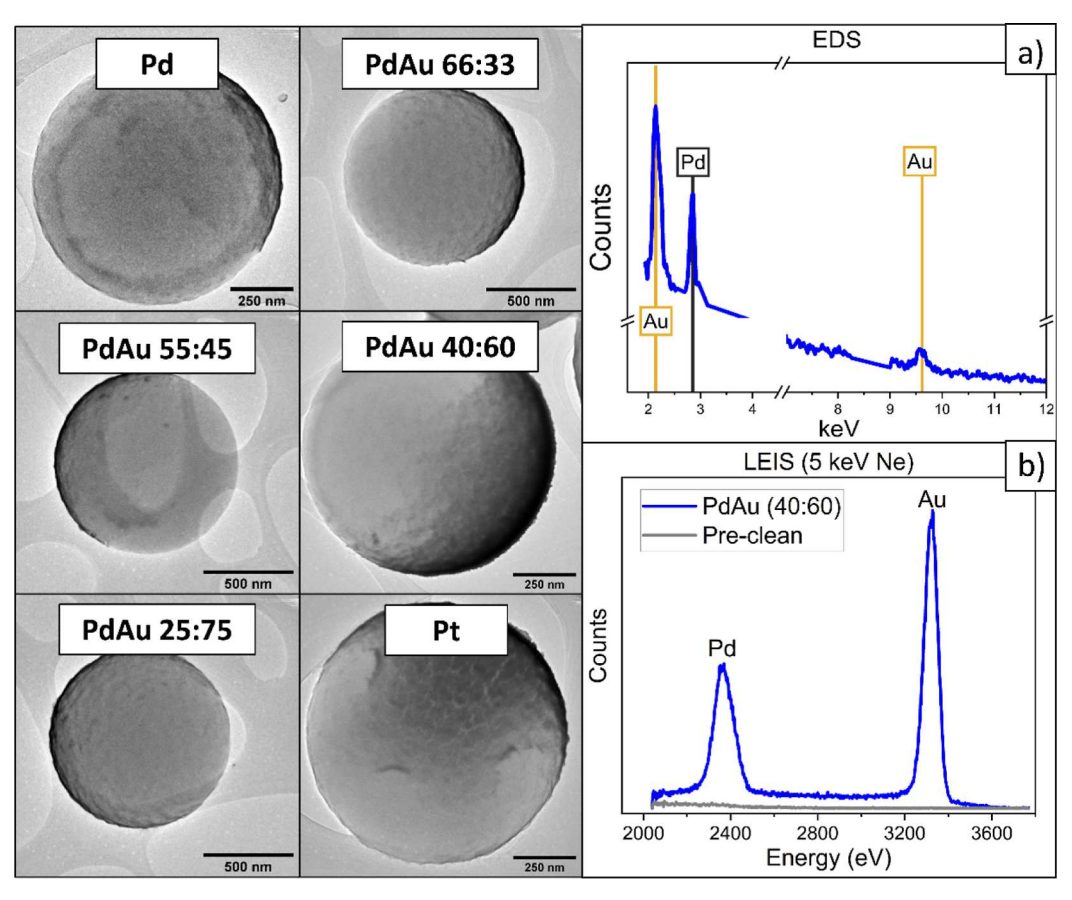


Figure 1. Representative TEM images of the synthesized particles. Representative spectra of characterization techniques used: (a) EDS data for PdAu 55:45 and (b) LEIS data for PdAu 40:60.

2.3. Data Analysis. Spatio-temporal trajectories (x, y, and z localizations vs elapsed time) were generated from the movies using DH-TRAX software, and the particle dynamics were quantified by calculating the time-averaged two-dimensional (2D) lateral mean-square displacement (MSD) of the trajectories. The z-component of trajectories were used to confirm the presence of active motion because self-propelled particles are known to exhibit approximate 2D trajectories in the presence of a planar surface. The passive 2D translational diffusion coefficient $D_{\rm T}$ was first experimentally determined by fitting the MSD data (Δr^2) versus lag time Δt to expression 1 for passive particle dynamics exhibited in the absence of H_2O_2 at each solution composition (i.e., each measured adsorbate concentration).

$$\Delta r^2 = 4D_{\rm T}\Delta t \tag{1}$$

All measured $D_{\rm T}$ values (and associated rotational diffusion coefficients, $D_{\rm R}$, and characteristic rotational time scales, $\tau_{\rm R}$) are reported in Table S1. These $D_{\rm T}$ values were then used as a fixed parameter to extract the active particle swimming velocity V from active experiments (H_2O_2 present) at the corresponding solution compositions. At time scales short compared to the characteristic time for rotational diffusion ($\Delta t < \tau_{\rm R}$), the velocity V is commonly extracted from the ballistic regime of particle motion using expression 2, $^{2.5}$

$$\Delta r^2 = 4D_{\rm T}\Delta t + V^2 \Delta t^2 \tag{2}$$

However, the reduced inherent catalytic activity of some of the synthesized particles (notably certain PdAu compositions) and subsequent adsorbate-induced attenuation of the active particle motion resulted in the ballistic regime being subtle to observe at these short lag times. At lag times long compared to $\tau_{\rm R}$, particle rotation gradually randomizes the direction of propulsion and the active MSD is asymptotically linear with lag time, with a slope greater than that for passive particles. Thus, in order to better highlight the attenuating effect of adsorbate on the particle motion, the velocity was instead extracted from the slope of the MSD at lag times longer than the characteristic time for rotational diffusion ($\Delta t > \tau_{\rm R}$) using expression 3, ²⁵

$$\Delta r^2 = (4D_{\rm T} + V^2 \tau_{\rm R}) \Delta t \tag{3}$$

For the measured conditions, the characteristic time for particle rotation τ_R was determined to be approximately 0.7 s (corresponding to a rotational diffusion coefficient D_R of ~ 1.4 rad²/s) and expressions 1 and 3 were consequently fit using MSD data at lag times of 1–2 s. We note that the V values extracted using the short lag time fit 2 and long lag time fit 3 for the Pt particles (where the ballistic regime and activity differences were apparent at short lag times) showed excellent agreement (Figure S3). Thus, all velocities in this work were obtained using the long lag time fit (velocity and coverage values given in Table S2).

Effective adsorbate coverages (θ) were determined from the extracted velocities by comparing the observed velocity at a given adsorbate concentration (V) with the particle velocity in the absence of adsorbate (V_0) using expression 4

$$\theta = 1 - \frac{V}{V_0} \tag{4}$$

These extracted coverages (θ) were plotted against adsorbate concentration C to construct Langmuir adsorption isotherms expression 5

$$\theta = \theta_{\text{max}} \frac{K_{\text{a}}C}{1 + K_{\text{a}}C} \tag{5}$$

where $\theta_{\rm max}$ is maximum saturation coverage and $K_{\rm a}$ is the affinity of the adsorbate to the catalyst surfaces. The values of $\theta_{\rm max}$ and $K_{\rm a}$ were obtained by linearizing expression 5 [plotting C/θ vs C to yield a slope of $1/\theta_{\rm max}$ and an intercept of $1/(\theta_{\rm max}K_{\rm a})$].

Uncertainties for the particle velocity and coverage represent the standard error of the swimming velocity and subsequent uncertainty propagation, respectively.

The enthalpy of adsorption $\Delta H_{\rm ads}$ was computed in two ways. First, isotherms at three separate temperatures (294, 303, and 311 K) were measured for furfural adsorption on the Pt surface. This enabled application of the Van't Hoff relation, that is, plotting the natural log of concentration against reciprocal temperature $[\ln(C) vs 1/T]$ with the product of the slope and the gas constant R yielding the enthalpy of adsorption. The enthalpy of adsorption for Pt and the other surfaces was additionally extracted at a single temperature (311 K) by normalizing the adsorption isotherms (transforming the measured affinity K_a to an equilibrium constant $K_{\rm ads,eq}$) and estimating the adsorption entropy change $\Delta S_{\rm ads}$ to enable enthalpy extraction *viaexpression* 6.8 This derivation and the utilized values are further detailed in the Supporting Information.

$$\ln(K_{\text{ads},\text{eq}}) = \frac{-\Delta G_{\text{ads}}}{RT} = \frac{-\Delta H_{\text{ads}}}{RT} + \frac{\Delta S_{\text{ads}}}{R}$$
(6)

3. RESULTS AND DISCUSSION

3.1. Synthesis of Active Particles with Varying **Surface Composition.** Active Janus particles (1 μ m diameter) were synthesized with caps of different metal compositions deposited on approximately one-half of the particle. Pt and Pd were deposited by sputtering from pure Pt and Pd targets, respectively. PdAu alloy caps were obtained by adhering gold discs to a Pd target, creating bimetallic sputter targets as described in the Methods section. As shown in Figure 1, sputtering both the neat metals as well as the alloys resulted in asymmetric metal deposition on the particle surface. To better highlight the asymmetric metal deposition, an aliquot of the capped particles was heated to 200 °C for 2 h to selectively melt the 1 μ m polystyrene particles; the remaining metal caps clearly resembled half-shells (Figure S4). The asdeposited composition of the metal caps was first analyzed using EDS to determine the bulk composition (representative EDS spectra showing Pd and Au peaks included in Figure 1a, full spectrum included in Figure S5), which confirmed the deposition of distinct PdAu alloys (Pd/Au ratios of 66:33, 55:45, 40:60, and 25:75). Furthermore, elemental mapping using EDS showed no evidence of obvious segregation of the metals, suggesting random alloying of the sputtered metals. As the outermost atoms are the most salient for controlling the binding of adsorbates, 28 LEIS was used to further analyze the composition and to selectively probe the composition of the outermost atomic layer (Figure 1b). Similar Pd/Au compositions were measured using LEIS and EDS on the PdAu 40:60

surface, suggesting the lack of selective enrichment of Pd or Au on the surface.

3.2. Activity of Synthesized Active Particles. The dynamics of the synthesized particles were investigated near to the surface of a clean glass substrate. As metal cap thickness can influence particle velocities, the same batch of each type of synthesized particles was used for all experiments. The synthesized particles all displayed active motion in peroxide fuel solutions; however, large metal-dependent differences in activity were observed. As shown in Figure 2, at 311 K in a

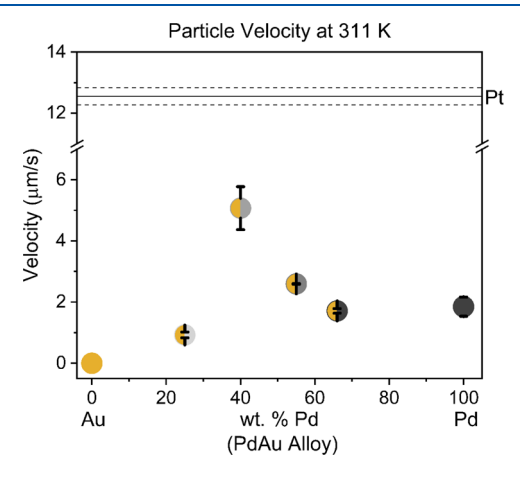


Figure 2. Symbols represent the velocity of PdAu alloy active particles in $10\% \ H_2O_2$ solution at 311 K. The dashed line shows the activity of Pt particles under the same conditions (the dashed lines indicate experimental uncertainties).

10% H₂O₂ solution, the particles with Pt metal exhibited rapid motion with swimming velocities greater than 12 μ m/s, more than twice the activity of the next most active metal composition. Classic characteristics of active motion were further exhibited by the Pt particles, namely, an observed ballistic regime in the MSD at short lag times and pronounced quasi-2D motion near the solid-liquid interface.²⁹ These results were consistent with literature reports; it is wellestablished that Pt coatings make for excellent active particles. Though less pronounced than Pt, the other metals (Pd and the PdAu alloys) also displayed active motion with velocities ranging from ~ 1 to 5 μ m/s (Figure 2), indicating that each metal composition decomposed H2O2 at time scales rapid enough to induce measurable particle motion. The alloy composition also impacted the activity, with the highest observed activity observed for the PdAu 40:60 alloy $(5.1 \ \mu \text{m/s})$. Interestingly, the pure Pd surface exhibited less activity (1.9 μ m/s), suggesting synergistic effects of Pd and Au for H₂O₂ decomposition. As expected, activity also decreased at high Au content; for example, the activity was only 0.9 μ m/s for the PdAu 25:75 alloy. More Pd-rich alloys (55:45 and 66:33 PdAu) displayed values of activity (2.6 and 1.7 μ m/s, respectively), approaching that of the pure Pd particles, potentially indicating that the synergistic effects on H₂O₂ decomposition were less pronounced as the surface increasingly resembled neat Pd. A wealth of literature has centered on PdAu alloys and H2O2 with particular interest toward the use of PdAu alloys as catalysts for direct synthesis of H₂O₂.²³ Interestingly, while some prior studies have suggested a monotonic increase in H₂O₂ selectivity with Au content in PdAu alloys, other work has identified PdAu ratios of 2:1 as

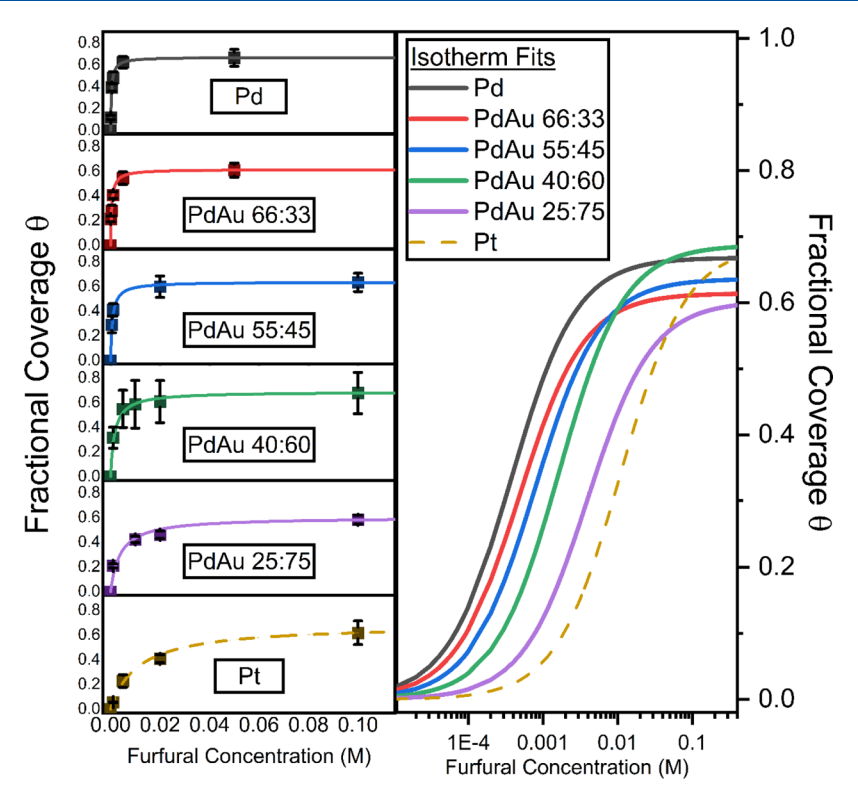


Figure 3. Apparent adsorption isotherms for furfural on each metal surface. Symbols represent experimental data, and the lines show the calculated fit to a Langmuir isotherm. The right panel shows the isotherm fits combined on a common semi-logarithmic scale.

optimal for H_2O_2 yield.^{32–34} These previously observed trends support the observations in the current work of a lower H_2O_2 decomposition rate (often correlated with higher selectivity during H_2O_2 synthesis) of the Pd/Au 66:33 alloy particles. We note, however, that direct comparison may be complicated by the nature of the metal in each study: the active particles featured a sputtered film of metal while the majority of direct H_2O_2 synthesis studies utilized metal nanoparticles.

As previously reported, the qualitative aspects of active motion were observed to be activity-dependent. While for the most active Pt particles a ballistic MSD regime was readily observed, as the particle activity decreased with changing metal compositions, the MSD at short lag times became increasingly linear as expected; indeed, for the least active PdAu 25:75 particles, the MSD at short lag times was indistinguishable from linear. However, the apparent mobility in this regime was measurably greater than for passive particles in the absence of fuel, which allowed for the quantitative determination of the active velocity from the long lag-time behavior, as described in the Materials section. Similarly, pronounced quasi-2D motion (another characteristic of active motion) was displayed by the active Pt particles. Moreover, decreasing activity resulted in increasing fluctuations in the z-direction as expected. We note that adsorption of organic compounds on pure Au surfaces is catalytically relevant; 35,36 however, synthesized Janus particles with pure Au caps displayed no activity in H₂O₂ solution and consequently were excluded from further adsorbate-attenuated motion analysis.

3.3. Quantitative Analysis of Adsorbate-Attenuated Active Motion. The effect of surface composition on organic adsorption was quantitatively probed by incubating the synthesized active particle with increasing concentrations of furfural. Furfural is an attractive candidate to probe the

differences in binding between different metal surfaces with furfural serving as both a commercially viable compound as well as a convenient analogue to understand the binding of other biomass-derived aromatic oxygenates. As previously reported, furfural and other organic adsorbates systematically attenuated active motion for Pt-coated particles. This reduction in active motion was attributed to physical occlusion of the metal active sites by adsorbed furfural that blocked access of the $\rm H_2O_2$ fuel. It was found that this attenuation of velocity could be quantitively linked to the adsorbed coverage of furfural and the adsorption process could be modeled using a Langmuir isotherm, enabling extraction of salient parameters of the adsorption process including the affinity and the maximum saturation coverage.

Increasing amounts of furfural in the mM regime were observed to attenuate the activity of the Pd and PdAu alloy particles, with the MSD of the particles systematically decreasing with increasing furfural concentrations (Figure S6). The velocities extracted from the MSD at each condition were recast as apparent fractional adsorbate coverage and used to construct isotherms for furfural adsorption on each metal surface (Figure 3). A qualitatively similar behavior was observed for all metal compositions, with rapid initial adsorption, followed by apparent saturation behavior. Interestingly, for all surfaces, this saturation did not approach unity, indicating that the furfural was not able to fully occlude the surface from access by H₂O₂ in the tested concentration range. Rather, all surfaces appeared to saturate between approximately 60-70% of full coverage. In the limit of infinite furfural chemical potential, full coverage of all surface sites should be achieved. We conclude that for all surfaces, there is a population of sites that bind furfural more weakly; this could be due to repulsive interactions with neighboring furfural adsorbates.³⁷ Furthermore, the rough sputtered surface of the metal caps may create significant heterogeneity in sites and access for different types of reactants and the observed plateau may be due to the saturation of the active sites to which the adsorbate has the highest affinity.

To quantify the relative strength of binding as a function of metal composition, the measured isotherms for each surface were fit to a Langmuir isotherm to extract the affinity of furfural to the different surfaces. The substantial differences in affinities (Table 1) show the dependence of furfural binding in

Table 1. Extracted Adsorption Parameters at 311 K

	affinity K_a (mM ⁻¹)
Pd	2.6 ± 0.2
PdAu 66:33	2.07 ± 0.03
PdAu 55:45	1.28 ± 0.07
PdAu 40:60	0.61 ± 0.05
PdAu 25:75	0.3 ± 0.1
Pt	0.09 ± 0.01

the liquid phase on the metal surface composition. In particular, suppression of active motion by furfural was much stronger on Pd than Pt (affinities of $2.6 \pm 0.2 \text{ vs } 0.09 \pm 0.01 \text{ mM}^{-1}$), with corresponding significantly higher coverages of adsorbate on the Pd surface than the Pt surface at similar furfural concentrations. On the alloyed surfaces, increasing Pd content also corresponded to increasing affinities (affinities: PdAu 66:33 > PdAu 55:45 > PdAu 40:60 > PdAu 25:75). Even the most Pd-lean alloy (PdAu 25:75) appeared to have a higher affinity for furfural than the Pt surface, further showing the key importance of metal on the binding. Notably, the affinity parameters did not simply show the same trend as the activity for H_2O_2 decomposition, which exhibited a maximum at intermediate Au content.

No clear correlation was apparent between the extracted affinities and the observed maximum coverages. For example, while Pd had a higher affinity and greater saturation coverage than the PdAu 66:33 alloy, Pt exhibited a substantially reduced affinity but also saturated at a higher coverage. This lack of correlation between affinity and saturation coverage suggested that competitive dynamic exchange of $\rm H_2O_2/\rm H_2O$ and the adsorbate was less likely to fully explain the observed trend in incomplete saturation coverage; rather, other mechanisms such as strong repulsive interactions at fractional coverages above 0.6 may be involved, particularly given the lack of dependence on surface composition.

3.4. Enthalpy of Adsorption. As described in the Methods section, the enthalpy of adsorption for furfural on the Pt surface was extracted using two approaches. As previously reported, three adsorption isotherms for furfural on Pt were constructed at different temperatures (294, 303, and 311 K). Per the Van't Hoff relation, the natural log of furfural concentration at the same coverages was plotted against reciprocal temperature to yield the enthalpy of adsorption of furfural on Pt as a function of coverage. 1 technique was complemented with another method - using the measured adsorption equilibrium constant and an estimate of the entropy of adsorption to extract enthalpies from adsorption isotherms.8 Briefly, the extracted affinity of furfural for the Pt surface was normalized and recast as an adsorption equilibrium constant. Henry's law was used to convert this equilibrium constant into the free energy of adsorption of the

gas-phase organic compound, which, coupled with an estimate of adsorption entropy, enabled extraction of the enthalpy of adsorption (parameters collected in Table S3). Both techniques have advantages. Using the three isotherms and Van't Hoff relation allows for extraction of the enthalpy using only experimental data, avoiding the need for estimates of entropy. Using the equilibrium constant and entropy estimate, however, only requires a single isotherm at one temperature. We found excellent agreement between methods: at equivalent coverages ($\theta = 0.054$), the Van't Hoff relation technique yielded an enthalpy of 69 ± 4 kJ/mol obtained via the equilibrium and entropy technique.

Constructing a series of temperature-dependent isotherms for each metal surface to extract the enthalpy *via* both strategies is appealing; however, the low inherent activity of the Pd and PdAu alloy particles complicated accurate measurement of adsorbate attenuation at temperatures lower than 311 K. Thus, the extracted enthalpies in Figure 4 were all derived using the second strategy.

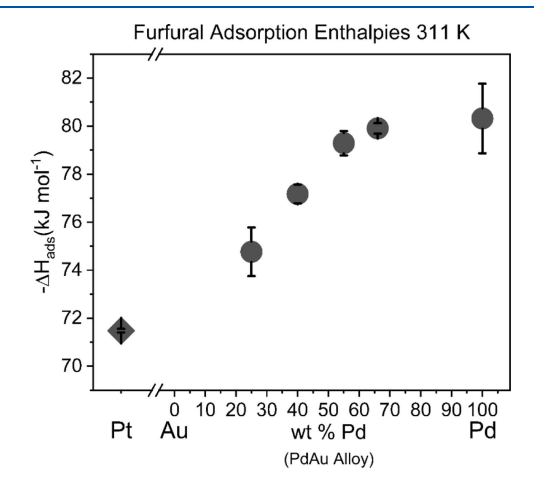


Figure 4. Enthalpy of adsorption as function of surface composition.

As shown in Figure 4, the enthalpy of adsorption for furfural on Pd was 80 ± 1 kJ/mol, approximately 10 kJ/mol stronger compared to adsorption on the Pt surface (71.5 \pm 0.1 kJ/mol). Interestingly, these values were significantly less than adsorption energies calculated in vacuum (~130 and 190 kJ/ mol of Pd and Pt, respectively, 16 tabulated in Table S4), consistent with the view that water layers on the catalytic surface dramatically weaken the enthalpic driving force for adsorption.³⁸ However, both the observed stronger binding on Pd surface compared to Pt and the relatively smaller difference of only ~10 kJ/mol stand somewhat in contrast to the computationally predicted stronger furfural binding on Pt versus Pd surfaces (Table S5). While we note that a difference of only 10 kJ/mol can still induce significant effects in reactivity, if the solvent effect on binding strength in the liquid phase was uniform between metal surfaces, one might expect a similar large difference (60 kJ/mol) in binding strength between the Pd and Pt surfaces in the liquid phase (albeit with lower overall magnitudes of each binding strength). Thus, the significantly smaller energy difference potentially suggests that the solvent effect energy correction may instead be metaldependent. Notably, computational studies have predicted nuanced facet-specific differences in furfural binding: for example, Pt binds furfural more strongly than Pd on (111)

facets but less strongly than Pd in some configurations on (110) surfaces.¹⁷ Moreover, other experimental results better corroborate the results in this work with experimental studies in ultra-high vacuum showing desorption of furfural at similar temperatures (365 K) on Pt *versus* Pd(111) surfaces, ^{14,37} suggesting more comparative binding strengths. We note that the rough morphology of the sputtered surface and presence of liquid, while relevant to many catalytic processes, may perturb adsorption processes compared to smooth surfaces in vacuum that complicate direct comparisons.

Similar to the measured affinities, the enthalpy of adsorption for the most Pd-lean alloy (PdAu 25:75) was greater in magnitude than for the Pt surface (75 \pm 1 vs 71.5 \pm 0.1 kJ/ mol). The magnitude of the measured adsorption enthalpy further increased monotonically with increasing Pd content in the PdAu alloys, consistent with computational calculations that predicted increasing Pd content in PdAu alloys leads to stronger binding of benzyl alcohol and gives rise to volcano plots for benzyl alcohol reactivity on these surfaces. 24,39 Introduction of Au into Pd surfaces can modify adsorbate binding through both electronic and geometric effects. 40 For example, Au has been suggested as an electron promotor in alloys and the formation of Pd-Au surface ensembles has been implicated in enhancing catalytic activity. Interestingly, these increases in catalytic activity for PdAu alloys have also been previously attributed to weakening of adsorption strength compared to pure Pd that increases free surface sites. 41 While furfural can bind to both Pd and Au surfaces, the observed decrease in binding energy with increasing Au content is consistent with previous reports and potentially suggests that Pd sites preferentially bind furfural stronger than Au sites in the alloy surface. Thus, increasing Au content in the alloy may decrease binding strength through dilution of the strongbinding Pd sites. Indeed, at intermediate PdAu compositions, the observed adsorption enthalpy for furfural appeared to trend linearly with Pd content, strikingly similar to the nearly linear calculated increase in H binding with increasing Pd content on PdAu surfaces. 19

At higher Pd contents (PdAu 66:33), the linear increase in enthalpy appeared to taper off to more closely resemble the energetics on the pure Pd surface. This further potentially suggests a predominant influence of Pd sites on the observed binding with the adsorption strength, where the binding strength initially increases rapidly with the introduction of more Pd sites in Pd-lean and intermediate compositions. At Pd-rich compositions, however, islands of Pd may form on the active surface that dominate the observed binding, leading to an observed adsorption strength that approaches that of the pure Pd surface more gradually. This is consistent with a prior observation that shows contiguous Pd islands exhibit high activity for benzyl alcohol activation.

We note that the applicability of this technique to probe furfural adsorption is predicated on blocking sites that are active for H_2O_2 decomposition. Interestingly, the maximum particle velocity induced by H_2O_2 decomposition is at intermediate PdAu compositions, whereas pure Pd binds furfural with the highest energy. The divergence in these trends is not necessarily surprising, but highlights the fact that distribution of sites on the surface changes as Pd composition is increased, and that the activity of various bimetallic sites differ substantially. Thus, the adsorption energies reported in Figure 4 represent an average adsorption energy across the sites that are active for H_2O_2 decomposition, and one must

bear in mind that this site dependence may differ for other reactions. As there appears to be compositional site dependence for H_2O_2 decomposition and limited reactivity on pure Au surfaces, furfural adsorption on more Pd-rich surfaces may suppress H_2O_2 decomposition more than similar adsorbed amounts of furfural on a surface with more contiguous Au sites. Weakening of adsorption strength has been implicated in increasing catalytic activity on PdAu alloy surfaces compared to pure Pd surfaces; ⁴¹ thus, the maximum rate of H_2O_2 decomposition observed at intermediate PdAu compositions may result from increased amounts of free surface sites available due to the weaker binding of H_2O_2 on the alloyed surfaces.

The overall change in adsorption enthalpy observed over the range of PdAu alloys (PdAu 25:75 to pure Pd) was only ~5 kJ/mol, significantly less than the energy differences predicted by some calculations: for example, benzyl alcohol adsorption in vacuum on a pure Pd surface and a PdAu 75:25 surface were predicted to vary by more than 35 kJ/mol,²⁴ while H binding energy in vacuum was calculated to range almost 50 kJ/mol as Pd content increased from 30 to 100% in PdAu alloys. 19 While significant reductions in the magnitude of vacuum-predicted adsorption energies are expected in the liquid-phase,⁵ the results from this work potentially suggest that the solventmediated energy changes are not uniform between metals as the absolute range of binding energies for the PdAu surfaces appears to significantly contract (~5 kJ/mol) compared to the ranges predicted in vacuum (35-50 kJ/mol). The overall trends in binding strength hold: the higher the Pd content, the stronger the binding of aromatic oxygenates (furfural and benzyl alcohol) in both vacuum and the gas phase.

It is important to note that the present study provides information only on overall adsorption energy trends, and not on the detailed mechanism for furfural adsorption on monometallic or bimetallic catalysts. Such information in principle can be provided by vibrational spectroscopy studies at the metal-water interface. For example, Hasse et al. 43 have employed surface-enhanced infrared spectroscopy to investigate furfural adsorption and electro-oxidation on Pt surfaces. They found that furfural adsorption was accompanied by some CO surface formation at low potentials, and that high (oxidizing) potentials led to surface oxidation of furfural to furoic acid and other surface-bound products. Román et al. 15 used similar techniques on Au electrodes and found that furfural can switch from a more flat-lying to more upright intermediate at higher oxidative potentials. However, the best opportunity for obtaining a detailed understanding of adsorption mechanism is likely through computational studies. Our previous work on Pt showed excellent agreement between furfural adsorption energies determined by active particle measurements and density functional studies employing an aqueous solution model.¹³ The DFT studies suggested that at low-temperature conditions with no applied potential, furfural adsorbs in a flat-lying configuration on Pt(111), and furthermore that competition with water for active sites results in a significant lowering of the effective strength of adsorption compared to the vacuum-Pt interface. Further computational studies of bimetallic surfaces are needed to translate the adsorption energy trends discussed here for PdAu systems to molecular-scale surface-adsorbate interactions.

4. CONCLUSIONS

In this study, we probed liquid-phase furfural adsorption on a range of metal substrates including Pt, Pd, and various PdAu bimetallics. Janus colloids with caps of each metal were synthesized, and the reduction in observed velocity as a function of furfural concentration was leveraged to construct adsorption isotherms for furfural on each metal substrate. Pd sites were shown to strongly bind furfural with the surface affinity of furfural increasing monotonically with increasing Pd content in the alloyed surfaces and reaching a maximum of 2.6 ± mM⁻¹ for the pure Pd surface. These measured affinities were further used to extract the enthalpy of adsorption for furfural on each surface, a quantity that is significant to the understanding and design of catalytic systems but traditionally challenging to determine in the presence of solvent. We find that Pd binds furfural more strongly than Pt in the liquid phase by nearly 10 kJ/mol. Furthermore, similar to the measured affinities, the enthalpy of adsorption for furfural increased with Pd content, suggesting that Pd sites act to control furfural binding on PdAu alloys. The relative strength of binding energies between surfaces has important consequences in catalysis in controlling adsorption, relative coverages, and reaction rates. This work shows how the adsorption energies can be directly probed in the liquid phase using active particle dynamics to better elucidate the effect of the metal composition on organic binding in the liquid phase.

ASSOCIATED CONTENT

Supporting Information

The Supporting Information is available free of charge at https://pubs.acs.org/doi/10.1021/acs.jpcc.2c05907.

Extended description of materials and methods; detailed information on particle dynamics; particle images; and determination of adsorption enthalpies (PDF)

AUTHOR INFORMATION

Corresponding Authors

J. Will Medlin — Department of Chemical and Biological Engineering, University of Colorado, Boulder, Colorado 80309, United States; orcid.org/0000-0003-2404-2443; Email: medlin@colorado.edu

Daniel K. Schwartz — Department of Chemical and Biological Engineering, University of Colorado, Boulder, Colorado 80309, United States; orcid.org/0000-0001-5397-7200; Email: daniel.schwartz@colorado.edu

Author

Benjamin Greydanus — Department of Chemical and Biological Engineering, University of Colorado, Boulder, Colorado 80309, United States; orcid.org/0000-0003-4954-3180

Complete contact information is available at: https://pubs.acs.org/10.1021/acs.jpcc.2c05907

Notes

The authors declare no competing financial interest.

ACKNOWLEDGMENTS

This work was supported by the Department of Energy, Office of Science, Basic Energy Sciences Program, Chemical Sciences, Geosciences, and Biosciences Division [grant no. DE-SC0005239]. The imaging was performed at the BioFrontiers

Institute Advanced Light Microscopy Core, and microscopy was performed on a Nikon Ti-E microscope supported by the Howard Hughes Medical Institute. This research was also supported in part by the Colorado Shared Instrumentation in Nanofabrication and Characterization (COSINC) and the CU Facility for Electron Microscopy of Materials (CUFEMM). B.G. acknowledges the Graduate Assistance in Areas of National Need Fellowship and the Department of Education for financial assistance.

REFERENCES

- (1) Crossley, S.; Faria, J.; Shen, M.; Resasco, D. E. Solid Nanoparticles That Catalyze Biofuel Upgrade Reactions at the Water/Oil Interface. *Science* **2010**, 327, 68–72.
- (2) Greydanus, B.; Schwartz, D. K.; Medlin, J. W. Controlling Catalyst-Phase Selectivity in Complex Mixtures with Amphiphilic Janus Particles. *ACS Appl. Mater. Interfaces* **2020**, *12*, 2338–2345.
- (3) Dyson, P. J.; Jessop, P. G. Solvent Effects in Catalysis: Rational Improvements of Catalysts: Via Manipulation of Solvent Interactions. *Catal. Sci. Technol.* **2016**, *6*, 3302–3316.
- (4) Li, G.; Wang, B.; Resasco, D. E. Water-Mediated Heterogeneously Catalyzed Reactions. ACS Catal. 2020, 10, 1294–1309.
- (5) Singh, N.; Campbell, C. T. A Simple Bond-Additivity Model Explains Large Decreases in Heats of Adsorption in Solvents Versus Gas Phase: A Case Study with Phenol on Pt(111) in Water. ACS Catal. 2019, 9, 8116–8127.
- (6) Montemore, M. M.; Medlin, J. W. Scaling Relations between Adsorption Energies for Computational Screening and Design of Catalysts. *Catal. Sci. Technol.* **2014**, *4*, 3748–3761.
- (7) Park, J.; Roling, L. T. Elucidating Energy Scaling between Atomic and Molecular Adsorbates in the Presence of Solvent. *AIChE J.* **2020**, *66*, No. e17036.
- (8) Akinola, J.; Barth, I.; Goldsmith, B. R.; Singh, N. Adsorption Energies of Oxygenated Aromatics and Organics on Rhodium and Platinum in Aqueous Phase. ACS Catal. 2020, 10, 4929–4941.
- (9) Gileadi, E. Electrosorption of Uncharged Molecules on Solid Electrodes. J. Electroanal. Chem. 1966, 11, 137–151.
- (10) Chen, X.; Zhou, C.; Wang, W. Colloidal Motors 101: A Beginner's Guide to Colloidal Motor Research. *Chem. Asian J.* **2019**, 14, 2388–2405.
- (11) Wu, H.; Greydanus, B.; Schwartz, D. K. Mechanisms of Transport Enhancement for Self-Propelled Nanoswimmers in a Porous Matrix. *Proc. Natl. Acad. Sci. U.S.A.* **2021**, *118*, No. e2101807118.
- (12) Ebbens, S. J.; Gregory, D. A. Catalytic Janus Colloids: Controlling Trajectories of Chemical Microswimmers. *Acc. Chem. Res.* **2018**, *51*, 1931–1939.
- (13) Greydanus, B.; Saleheen, M.; Wu, H.; Heyden, A.; Medlin, J. W.; Schwartz, D. K. Probing Surface-Adsorbate Interactions through Active Particle Dynamics. *J. Colloid Interface Sci.* **2022**, *614*, 425–435.
- (14) Mark, L. O.; Jenkins, A. H.; Heinz, H.; Medlin, J. W. Furfuryl Alcohol Deoxygenation, Decarbonylation, and Ring-Opening on Pt(111). Surf. Sci. 2018, 677, 333–340.
- (15) Román, A. M.; Agrawal, N.; Hasse, J. C.; Janik, M. J.; Medlin, J. W.; Holewinski, A. Electro-Oxidation of Furfural on Gold Is Limited by Furgate Self-Assembly. *J. Catal.* **2020**, *391*, 327–335.
- (16) Sivec, R.; Huš, M.; Likozar, B.; Grilc, M. Furfural Hydrogenation over Cu, Ni, Pd, Pt, Re, Rh and Ru Catalysts: Ab Initio Modelling of Adsorption, Desorption and Reaction Micro-Kinetics. *Chem. Eng. J.* **2022**, 436, 135070.
- (17) Khan, A. Z.; Alitt, J.; Germaney, R.; Hamada, I.; Wells, P. P.; Dimitratos, N.; Catlow, C. R. A.; Villa, A.; Chutia, A. A Comparative Study on the Stability of the Furfural Molecule on the Low Index Ni, Pd and Pt Surfaces. *R. Soc. Open Sci.* **2022**, *9*, 211516.
- (18) Bramley, G. A.; Nguyen, M. T.; Glezakou, V. A.; Rousseau, R.; Skylaris, C. K. Understanding Adsorption of Organics on Pt(111) in the Aqueous Phase: Insights from DFT Based Implicit Solvent and

- Statistical Thermodynamics Models. J. Chem. Theory Comput. 2022, 18, 1849–1861.
- (19) Kunal, P.; Li, H.; Dewing, B. L.; Zhang, L.; Jarvis, K.; Henkelman, G.; Humphrey, S. M. Microwave-Assisted Synthesis of PdxAu100-x Alloy Nanoparticles: A Combined Experimental and Theoretical Assessment of Synthetic and Compositional Effects upon Catalytic Reactivity. *ACS Catal.* 2016, 6, 4882–4893.
- (20) Huang, X.; Akdim, O.; Douthwaite, M.; Wang, K.; Zhao, L.; Lewis, R. J.; Pattisson, S.; Daniel, I. T.; Miedziak, P. J.; Shaw, G.; Morgan, D. J.; Althahban, S. M.; Davies, T. E.; He, Q.; Wang, F.; Fu, J.; Bethell, D.; McIntosh, S.; Kiely, C. J.; Hutchings, G. J. Au-Pd Separation Enhances Bimetallic Catalysis of Alcohol Oxidation. *Nature* 2022, 603, 271–275.
- (21) Li, H.; Guo, S.; Shin, K.; Wong, M. S.; Henkelman, G. Design of a Pd-Au Nitrite Reduction Catalyst by Identifying and Optimizing Active Ensembles. *ACS Catal.* **2019**, *9*, 7957–7966.
- (22) Seraj, S.; Kunal, P.; Li, H.; Henkelman, G.; Humphrey, S. M.; Werth, C. J. PdAu Alloy Nanoparticle Catalysts: Effective Candidates for Nitrite Reduction in Water. *ACS Catal.* **2017**, *7*, 3268–3276.
- (23) Ricciardulli, T.; Gorthy, S.; Adams, J. S.; Thompson, C.; Karim, A. M.; Neurock, M.; Flaherty, D. W. Effect of Pd Coordination and Isolation on the Catalytic Reduction of O2to H2O2over PdAu Bimetallic Nanoparticles. *J. Am. Chem. Soc.* **2021**, *143*, 5445–5464.
- (24) Wu, P.; Cao, Y.; Zhao, L.; Wang, Y.; He, Z.; Xing, W.; Bai, P.; Mintova, S.; Yan, Z. Formation of PdO on Au–Pd Bimetallic Catalysts and the Effect on Benzyl Alcohol Oxidation. *J. Catal.* **2019**, 375, 32–43.
- (25) Howse, J. R.; Jones, R. A. L.; Ryan, A. J.; Gough, T.; Vafabakhsh, R.; Golestanian, R. Self-Motile Colloidal Particles: From Directed Propulsion to Random Walk. *Phys. Rev. Lett.* **2007**, *99*, 048102.
- (26) Guo, X.; Wang, J. Comparison of Linearization Methods for Modeling the Langmuir Adsorption Isotherm. *J. Mol. Liq.* **2019**, 296, 111850.
- (27) Nuhnen, A.; Janiak, C. A Practical Guide to Calculate the Isosteric Heat/Enthalpy of Adsorption: Via Adsorption Isotherms in Metal-Organic Frameworks, MOFs. *Dalton Trans.* **2020**, *49*, 10295–10307
- (28) Li, H.; Shin, K.; Henkelman, G. Effects of Ensembles, Ligand, and Strain on Adsorbate Binding to Alloy Surfaces. *J. Chem. Phys.* **2018**, *149*, 174705.
- (29) Ketzetzi, S.; de Graaf, J.; Kraft, D. J. Diffusion-Based Height Analysis Reveals Robust Microswimmer-Wall Separation. *Phys. Rev. Lett.* **2020**, *125*, 238001.
- (30) Das, S.; Garg, A.; Campbell, A. I.; Howse, J.; Sen, A.; Velegol, D.; Golestanian, R.; Ebbens, S. J. Boundaries Can Steer Active Janus Spheres. *Nat. Commun.* **2015**, *6*, 8999.
- (31) Jalilvand, Z.; Pawar, A. B.; Kretzschmar, I. Experimental Study of the Motion of Patchy Particle Swimmers Near a Wall. *Langmuir* **2018**, *34*, 15593–15599.
- (32) Ouyang, L.; Da, G. J.; Tian, P. F.; Chen, T. Y.; Liang, G.-D.; Xu, J.; Han, Y. F. Insight into Active Sites of Pd-Au/TiO2 Catalysts in Hydrogen Peroxide Synthesis Directly from H2 and O2. *J. Catal.* **2014**, *311*, 129–136.
- (33) Bernardotto, G.; Menegazzo, F.; Pinna, F.; Signoretto, M.; Cruciani, G.; Strukul, G. New Pd-Pt and Pd-Au Catalysts for an Efficient Synthesis of H2O2 from H2 and O2 under Very Mild Conditions. *Appl. Catal., A* **2009**, 358, 129–135.
- (34) Xu, H.; Cheng, D.; Gao, Y. Design of High-Performance Pd-Based Alloy Nanocatalysts for Direct Synthesis of H2O2. ACS Catal. 2017, 7, 2164–2170.
- (35) Jenkins, A. H.; Musgrave, C. B.; Medlin, J. W. Enhancing Au/TiO2 Catalyst Thermostability and Coking Resistance with Alkyl Phosphonic-Acid Self-Assembled Monolayers. *ACS Appl. Mater. Interfaces* **2019**, *11*, 41289–41296.
- (36) Quast, A. D.; Bornstein, M.; Greydanus, B. J.; Zharov, I.; Shumaker-Parry, J. S. Robust Polymer-Coated Diamond Supports for Noble-Metal Nanoparticle Catalysts. *ACS Catal.* **2016**, *6*, 4729–4738.

- (37) Pang, S. H.; Medlin, J. W. Adsorption and Reaction of Furfural and Furfuryl Alcohol on Pd(111): Unique Reaction Pathways for Multifunctional Reagents. *ACS Catal.* **2011**, *1*, 1272–1283.
- (38) Akinola, J.; Singh, N. Temperature Dependence of Aqueous-Phase Phenol Adsorption on Pt and Rh. J. Appl. Electrochem. **2021**, 51, 37–50.
- (39) Silva, T. A. G.; Teixeira-Neto, E.; López, N.; Rossi, L. M. Volcano-like Behavior of Au-Pd Core-Shell Nanoparticles in the Selective Oxidation of Alcohols. *Sci. Rep.* **2014**, *4*, 5766.
- (40) Liu, P.; Nørskov, J. K. Ligand and Ensemble Effects in Adsorption on Alloy Surfaces. *Phys. Chem. Chem. Phys.* **2001**, 3, 3814–3818.
- (41) Griffin, M. B.; Rodriguez, A. A.; Montemore, M. M.; Monnier, J. R.; Williams, C. T.; Medlin, J. W. The Selective Oxidation of Ethylene Glycol and 1,2-Propanediol on Au, Pd, and Au-Pd Bimetallic Catalysts. *J. Catal.* **2013**, 307, 111–120.
- (42) Wang, H.; Wang, C.; Yan, H.; Yi, H.; Lu, J. Precisely-Controlled Synthesis of Au@Pd Core-Shell Bimetallic Catalyst via Atomic Layer Deposition for Selective Oxidation of Benzyl Alcohol. *J. Catal.* **2015**, 324, 59–68.
- (43) Hasse, J. C.; Agrawal, N.; Janik, M. J.; Holewinski, A. ATR-SEIRAS Investigation of the Electro-Oxidation Mechanism of Biomass-Derived C5 Furanics on Platinum Electrodes. *J. Phys. Chem. C* 2022, 126, 7054–7065.

TRecommended by ACS

Ensemble Effects in Adsorbate-Adsorbate Interactions in Microkinetic Modeling

Elisabeth M. Dietze and Henrik Grönbeck

JANUARY 18, 2023

JOURNAL OF CHEMICAL THEORY AND COMPUTATION

READ 🗹

Development of Atomistic Kerogen Models and Their Applications for Gas Adsorption and Diffusion: A Mini-Review

Amaël Obliger, Jean-Marc Leyssale, et al.

JANUARY 13, 2023

ENERGY & FUELS

READ

In Vivo Fast Nonlinear Microscopy Reveals Impairment of Fast Axonal Transport Induced by Molecular Motor Imbalances in the Brain of Zebrafish Larvae

Baptiste Grimaud, François Treussart, et al.

DECEMBER 02, 2022

ACS NANO

READ 🗹

Unraveling the Molecular Interface and Boundary Problems in an Electrical Double Layer and Electroosmotic Flow

Md Masuduzzaman and BoHung Kim

MAY 27, 2022

LANGMUIR

READ 🗹

Get More Suggestions >